Chemical Engineering Journal 263 (2015) 101–112

Contents lists available at ScienceDirect

Chemical Engineering Journal

journal homepage: www.elsevier.com/locate/cej

Polyethersulfone membrane enhanced with iron oxide nanoparticles for copper removal from water: Application of new functionalized Fe_3O_4 nanoparticles

Negin Ghaemi [a,*], Sayed S. Madaeni [b], Parisa Daraei [a], Hamid Rajabi [b,c], Sirus Zinadini [d], Abdolhamid Alizadeh [e], Rouhollah Heydari [f], Mojtaba Beygzadeh [g], Sohrab Ghouzivand [e]

[a] *Department of Chemical Engineering, Kermanshah University of Technology, 67178 Kermanshah, Iran*
[b] *Membrane Research Centre, Department of Chemical Engineering, Razi University, Tagh Bostan, 67149 Kermanshah, Iran*
[c] *Department of Civil Engineering, Razi University, 67149 Kermanshah, Iran*
[d] *Water and Wastewater Research Center (WWRC), Department of Applied Chemistry, Faculty of Chemistry, Razi University, Kermanshah, Iran*
[e] *Department of Organic Chemistry, Faculty of Chemistry and Nanoscience & Nanotechnology Research Center (NNRC), Razi University, 67149 Kermanshah, Iran*
[f] *Razi Herbal Medicines Research Center, Lorestan University of Medical Sciences, 68149-89468 Khorramabad, Iran*
[g] *Department of Energy, Materials and Energy Research Center, 14155-4777 Tehran, Iran*

HIGHLIGHTS

- Fe_3O_4 nanoparticles were coated by silica, metformine and amine.
- PES membranes were enhanced by embedding modified Fe_3O_4 based nanoparticles (NPs).
- Embedding NPs affected on morphology and hydrophilicity of PES membranes.
- Water flux and copper removal of nano-enhanced membranes improved.
- The membrane enhanced with metformine coated NPs revealed the highest efficiency.

GRAPHICAL ABSTRACT

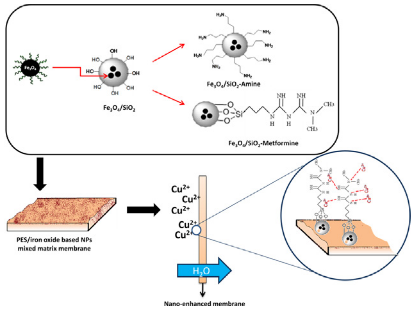

ARTICLE INFO

Article history:
Received 22 August 2014
Received in revised form 28 October 2014
Accepted 29 October 2014
Available online 4 November 2014

Keywords:
Nano-enhanced membrane
Iron oxide nanoparticles
Functionalized Fe_3O_4
Heavy metal
Copper ion removal

ABSTRACT

Surface modification of Fe_3O_4 nanoparticles was performed by immobilizing silica, metformine, and amine. Mixed matrix PES nanofiltration membrane was prepared by embedding various concentrations of the modified Fe_3O_4 based nanoparticles. The membranes were characterized in terms of morphology and performance including investigation of SEM and AFM microphotographs, water contact angle, mean pore size and porosity measurements and determination of pure water flux as well as copper ion removal. Embedding iron oxide nanoparticles resulted in a significant rise in the pure water flux as a result of changes in the mean pore radius, porosity and hydrophilicity of the membranes. Moreover, the copper removal capability of prepared membranes remarkably increased because of improved hydrophilicity and also presence of nucleophilic functional groups on nanoparticles. The membrane fabricated with 0.1 wt.% metformine-modified silica coated Fe_3O_4 nanoparticles showed the highest copper removal (about 92%) due to high affinity in copper adsorption. Moreover, acceptable reusability was found for the membrane with the best performance after several times of usage/regeneration cycles using EDTA as eluting agent.

---

* Corresponding author. Tel.: +98 83 37267530; fax: +98 83 37267540.
E-mail addresses: negin_ghaemi@kut.ac.ir, negin_ghaemi@yahoo.com (N. Ghaemi).

http://dx.doi.org/10.1016/j.cej.2014.10.103
1385-8947/

Nomenclature

Symbols & abbreviations

A	membrane area (m^2)
A'	surface of membrane sample (cm^2)
AFM	atomic force microscopy
APTES	3-aminopropyltriethoxysilane
C_f	copper ion concentration in feed (mg/l)
C_p	copper ion concentration in permeate (mg/l)
CPTS	3-chloropropyl-trimethoxysilane
DMAc	N,N-dimethylacetamide
d_w	water density (0.998 g/cm^3)
EDTA	ethylenediaminetetraacetic acid
EDX	energy dispersive X-ray spectroscopy
Fe_3O_4/SiO_2	silica-coated Fe_3O_4 nanoparticles
Fe_3O_4/SiO_2-Amine	amine-modified silica-coated Fe_3O_4 nanoparticles
Fe_3O_4/SiO_2-Met	metformin-modified silica-coated Fe_3O_4 nanoparticles
FT-IR	Fourier transform infrared spectroscopy
l	membrane thickness (cm)
K_2CO_3	potassium carbonate
KI	potassium iodide
NP	nanoparticle
NPs	nanoparticles
PES	polyethersulfone
PA6	polyamide 6
PES/Fe	PES membrane enhanced with Fe_3O_4 nanoparticles
PES/$Fe_{0.01}$	PES membrane enhanced with 0.01 wt.% Fe_3O_4 nanoparticles
PES/$Fe_{0.1}$	PES membrane enhanced with 0.1 wt.% Fe_3O_4 nanoparticles
PES/Fe_1	PES membrane enhanced with 1 wt.% Fe_3O_4 nanoparticles
PES/FeSi	PES membrane enhanced with silica-coated Fe_3O_4 nanoparticles
PES/$FeSi_{0.01}$	PES membrane enhanced with 0.01 wt.% Fe_3O_4/SiO_2 nanoparticles
PES/$FeSi_{0.1}$	PES membrane enhanced with 0.1 wt.% Fe_3O_4/SiO_2 nanoparticles
PES/$FeSi_1$	PES membrane enhanced with 1 wt.% Fe_3O_4/SiO_2 nanoparticles
PES/FeSiAmine	PES membrane enhanced with amine-modified silica-coated Fe_3O_4 nanoparticles
PES/$FeSiAmine_{0.01}$	PES membrane enhanced with 0.01 wt.% Fe_3O_4/SiO_2-Amine nanoparticles
PES/$FeSiAmine_{0.1}$	PES membrane enhanced with 0.1 wt.% Fe_3O_4/SiO_2-Amine nanoparticles
PES/$FeSiAmine_1$	PES membrane enhanced with 1 wt.% Fe_3O_4/SiO_2-Amine nanoparticles
PES/FeSiMet	PES membrane enhanced with metformin-modified silica-coated Fe_3O_4 nanoparticles
PES/$FeSiMet_{0.01}$	PES membrane enhanced with 0.01 wt.% Fe_3O_4/SiO_2-Met nanoparticles
PES/$FeSiMet_{0.1}$	PES membrane enhanced with 0.1 wt.% Fe_3O_4/SiO_2-Met nanoparticles
PES/$FeSiMet_1$	PES membrane enhanced with 1 wt.% Fe_3O_4/SiO_2-Met nanoparticles
PVP	polyvinylpyrrolidone
Q	quantity of permeate (kg)
Q'	volumetric flow rate of permeated pure water (m^3/s)
R (%)	removal of copper ion
r_m	membrane mean pore radius
S_a	mean roughness (nm)
SEM	scanning electron microscopy
S_q	root mean square of the Z data (nm)
S_z	mean difference between highest peaks and lowest valleys (nm)
TEM	transmission electron microscopy
TEOS	tetraethyl orthosilicate
TPEE/IO	thermal plastic elastomer ester/iron oxide
WCA	water contact angle (°)
W_d	dry membrane weight (g)
W_w	wet membrane weight (g)
XRD	X-ray diffraction
ε (%)	overall porosity
η	water viscosity (8.9×10^{-4} Pa s)
ΔP	operating pressure (0.4 MPa)
Δt	sampling time (h)

1. Introduction

Heavy metal ions must be eliminated from water resources due to their hazardous effects [1–4]. Hereupon, attempts for removal of heavy metals including copper ions, as a toxic metal ion, have been developed by several methods [5–9]. Many studies have focused on adsorptive removal of Cu(II) either by adsorbents or by membranes [10–13]. The outstanding characteristic of membranes made them a pioneer technology to be employed in this field. In this way, adsorptive membranes were prepared by blending some polymers such as cellulose acetate, acrylonitrile butadiene styrene and polyvinyl alcohol with an adsorptive polymer like chitosan to enhance adsorptive capability of membranes for heavy metal elimination from water [14–18].

Utilizing the nanoparticles in membrane preparation was also applied to improve adsorptive removal of heavy metals, especially copper using polymeric membranes. Meanwhile, metal oxide nanoparticles were widely used as an additive in order to optimize membrane performance [19]. Compared with other metal oxides, conspicuous impact of iron oxide nanoparticles on membranes performance for removal of metal ions was reported by researchers [18–22]. The observed results were attributed to the great affinity of iron oxides toward heavy metals [18].

Xu et al. [23] fabricated a hierarchically TPEE/IO nanofibrous membrane with easy solid/liquid separation properties by electrospinning and hydrothermal method. The obtained membrane showed excellent Cr(VI) removal efficiency. In another work [24] PA6@Fe_xO_y nanofibrous membranes were prepared by electrospinning and hydrothermal method. Such nanofibrous membranes exhibited excellent performance for Cr removal from $K_2Cr_2O_7$ solution using Freundlich adsorption mechanism. Polyvinylchloride-blend-cellulose acetate/iron oxide nanocomposite membranes were also prepared by casting technique. In this case, the nanocomposite membranes revealed higher water flux as well as superior lead removal compared with pristine membrane [23].

In addition to intrinsic adsorptive properties of metal oxide nanoparticles, they can be modified by other chemicals and can be coupled with desired functional groups to obtain nanoparticles with new properties and capabilities [18,25]. The adsorptive removal of copper ions was remarkably improved using mixed matrix PES membrane embedded with polyaniline modified Fe_3O_4 nanoparticles [18]. It was proved that NH groups of polyaniline were responsible for improving the adsorptive properties of Fe_3O_4 nanoparticles due to the presence of nitrogen atoms with a lone electron pair as a reactive site for adsorption of Cu(II) ions. However, the water flux of nanocomposite membranes decreased as a result of pore blockage by accumulated nanoparticles [18]. In order to solve problems regarding the flux reduction, it would be a good idea to employ iron oxide nanoparticles modified by materials with more hydrophilicity compared with previously applied modifiers like polyaniline.

The present study is an attempt to simultaneously increase the permeate flux and Cu(II) removal efficiency of PES membrane by increasing the hydrophilicity of modified iron oxide nanoparticles. Four types of iron oxide-based nanoparticles are synthesized and applied to probe the effect of functionalization of Fe_3O_4 nanoparticles on the surface and cross-section morphology, overall porosity, mean pore size, hydrophilicity, pure water flux, and Cu(II) removal efficiency of PES membrane. SEM, AFM, and water contact angle techniques are employed to characterize the nano-enhanced membranes and to explain the obtained results. The reusability of membranes is examined by using EDTA regenerator which has great affinity to chelate Cu(II) ion.

2. Experimental

2.1. Materials

List of chemicals used in this study is tabulated in Table 1. All chemicals were in analytical grade (assay ⩾ 99%). Distilled water was used throughout the experiments.

Table 1
Identification of chemicals.

Chemical	Supplier
Acetone	Merck, Germany
Acetonitrile	Merck, Germany
Ammonium hydroxide	Merck, Germany
3-Aminopropyltriethoxysilane (APTES)	Merck, Germany
3-Chloropropyl-trimethoxysilane (CPTS)	Merck, Germany
Dimethylacetamide (DMAc)	Merck, Germany
Ethanol	Merck, Germany
Iron (III) chloride hexahydrate	Merck, Germany
Iron (II) chloride tetrahydrate	Merck, Germany
Metformin hydrochloride	Sigma-Aldrich, USA
PES, Ultrason E6020P (MW = 58,000 g/mol)	BASF, Germany
PVP (MW = 25,000 g/mol)	Merck, Germany
Potassium carbonate (K_2CO_3)	Merck, Germany
Potassium iodide (KI)	Merck, Germany
Tetraethyl orthosilicate (TEOS)	Merck, Germany
Toluene	Merck, Germany
Trisodium citrate	Merck, Germany

2.2. Synthesis of nanoparticles

2.2.1. Synthesis of Fe_3O_4 nanoparticles

Iron oxide nanoparticles modified with citrate groups were prepared according to the reported procedure by Yang et al. [26]. Typically, iron (III) chloride hexahydrate (2.70 g, 10 mmol) and iron (II) chloride tetrahydrate (1 g, 5 mmol) were dissolved in distilled water (130 ml) in Ar atmosphere. Then, 11 ml of ammonium hydroxide (28%) was quickly added into the solution under rapid mechanical stirring (900 rpm), and then the mixture (pH 9.5) was heated up to 60 °C, while vigorously stirred by a mechanical stirrer for 1 h under Ar. Finally, after cooling to room temperature, the resultant nanoparticles were collected using a magnet and the collected magnetic solids were dispersed in 200 ml of trisodium citrate solution (0.3 M) and heated at 80 °C for 1 h. Then, the precipitates were collected using an external magnet and washed with acetone to remove remnant trisodium citrate. The schematic of Fe_3O_4 nanoparticles treated with trisodium citrate is presented in Fig. 1(a).

2.2.2. Synthesis of silica-coated Fe_3O_4 nanoparticles (Fe_3O_4/SiO_2)

In order to form a ferro fluid, following Stöber method with some modifications [27], Fe_3O_4 nanoparticles (1 g) were dispersed in 50 ml of distilled water by ultrasonic treatment (50 Hz) for 20 min. Subsequently, the resultant dispersion was centrifuged for 30 min to remove any larger or agglomerated particles. Then, 30 ml of acetone was added to the solution to precipitate out the nanoparticles. In this step, 0.5 g of the obtained black precipitates was dispersed in 25 ml of water to make a 2.0 wt.% solution of ferro fluid. 2 ml of ferro fluid was first diluted with water (40 ml), the resultant suspension and 5 ml of $NH_3{\cdot}H_2O$ were poured into 140 ml of ethanol with final pH 10.48 under vigorous stirring at 40 °C. Finally, under continuous mechanical stirring, 1 ml of TEOS diluted in ethanol (20 ml) was drop wise added to this suspension. The resultant suspension was stirred at room temperature for 14 h. The Fe_3O_4/SiO_2 nanoparticles were collected by magnetic separation and washed with ethanol and de-ionized water in sequence. The schematic of Fe_3O_4/SiO_2 nanoparticles is presented in Fig. 1(b).

2.2.3. Synthesis of metformin-modified silica-coated Fe_3O_4 nanoparticles (Fe_3O_4/SiO_2-Met)

First, chloropropyl-modified silica-coated nanoparticles were prepared following the modified procedure of Zeng et al. [28]. After 1 ml (5 mmol) of CPTS was dissolved in 100 ml of dried toluene, this mixture was added into 1 g of Fe_3O_4/SiO_2 and solution was stirred at 60 °C for 18 h. The chloropropyl-functionalized solid (Fe_3O_4/SiO_2-Cl) was washed with toluene, separated by a magnet, and dried in vacuum. The obtained magnetic solid was used in the following step to synthesize metformin-modified silica-coated Fe_3O_4 nanoparticles. The prepared Fe_3O_4/SiO_2-Cl (1 g) and KI (1.66 g, 10 mmol) were added into a solution of metformin hydrochloride (0.21 g, 5 mmol) and K_2CO_3 (10 mmol, 1.38 g) in acetonitrile (50 ml) in a round-bottom flask and the mixture was stirred under reflux condition for 5 h. The obtained solid was then magnetically collected from the solution and washed copiously with water/ethanol followed by drying at 80 °C for 6 h. The schematic of Fe_3O_4/SiO_2-Met nanoparticles is presented in Fig. 1(c).

2.2.4. Synthesis of amine-modified silica-coated Fe_3O_4 nanoparticles (Fe_3O_4/SiO_2-Amine)

The amine-modified silica-coated Fe_3O_4 nanoparticles were prepared by surface functionalization of Fe_3O_4/SiO_2 nanoparticles using APTES as a silylation agent [29]. Fe_3O_4/SiO_2 nanoparticles (1 g) and 50 ml of toluene were added to a 250-ml three-necked flask and then ultrasonically dispersed for 30 min. Then, 2 ml of APTES was added into the flask, and solution was stirred at 80 °C for 12 h. The resulting functionalized Fe_3O_4/SiO_2 nanoparticles were collected by a magnet, washed with ethanol and acetone several times and dried at 50 °C. The schematic of Fe_3O_4/SiO_2-Amine nanoparticles is presented in Fig. 1(d).

2.3. Fabrication of PES nano-enhanced membranes

Pristine PES membrane and PES nano-enhanced membranes prepared with different types of Fe_3O_4 and functionalized Fe_3O_4 nanoparticles were fabricated using conventional phase inversion method at room temperature (20 ± 2 °C). Composition of all casting solutions are presented in Table 2.

A casting solution containing PES (18 wt.%) dissolved in DMAc (solvent) was prepared using PVP (1 wt.%) as pore former by stirring at 400 rpm for 24 h. Addition of nanoparticles was done in a procedure similar to the previous study [18]. The obtained

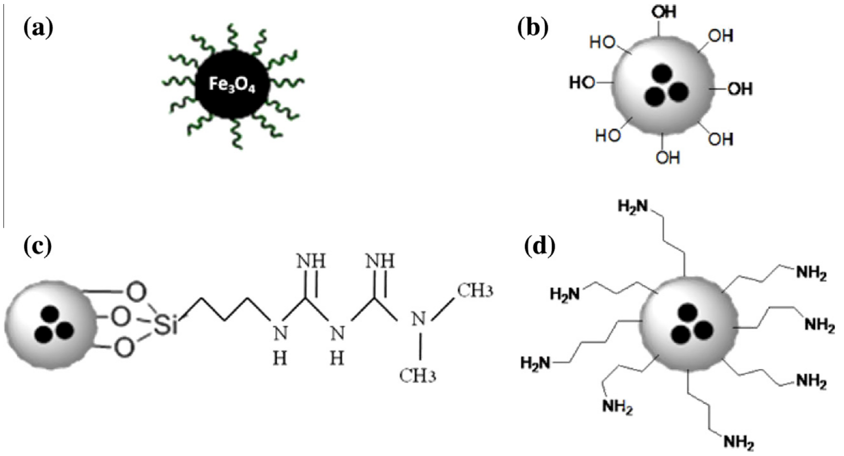

Fig. 1. Schematic of (a) Fe_3O_4 treated with trisodium citrate, (b) Fe_3O_4/SiO_2, (c) Fe_3O_4/SiO_2-Met and (d) Fe_3O_4/SiO_2-Amine nanoparticles.

Table 2
Composition of prepared membranes.

Name	PES (wt.%)	PVP (wt.%)	DMAc (wt.%)	Nanoparticle (wt.%)			
				Fe_3O_4	Fe_3O_4/SiO_2	Fe_3O_4/SiO_2-Met	Fe_3O_4/SiO_2-Amine
PES	18	1	81.00	–	–	–	–
PES/$Fe_{0.01}$	18	1	80.99	0.01	–	–	–
PES/$Fe_{0.1}$	18	1	80.90	0.10	–	–	–
PES/Fe_1	18	1	80.00	1.00	–	–	–
PES/$FeSi_{0.01}$	18	1	80.99	–	0.01	–	–
PES/$FeSi_{0.1}$	18	1	80.90	–	0.10	–	–
PES/$FeSi_1$	18	1	80.00	–	1.00	–	–
PES/$FeSiMet_{0.01}$	18	1	80.99	–	–	0.01	–
PES/$FeSiMet_{0.1}$	18	1	80.90	–	–	0.10	–
PES/$FeSiMet_1$	18	1	80.00	–	–	1.00	–
PES/$FeSiAmine_{0.01}$	18	1	80.99	–	–	–	0.01
PES/$FeSiAmine_{0.1}$	18	1	80.90	–	–	–	0.10
PES/$FeSiAmine_1$	18	1	80.00	–	–	–	1.00

homogeneous solution was casted on a glass plate using a homemade film applicator with 200 μm thickness. Distilled water was used as non-solvent for membrane preparation. After primarily phase separation and formation of membrane, it was kept in water for 24 h to guarantee complete phase separation and then, kept between filter papers to dry for another 24 h.

2.4. Characterization of membranes

2.4.1. Characterization methods

TEM imaging was conducted using a Philips CM10 equipped with a CCD camera. One drop of the sample suspension in water was deposited onto a copper substrate and the excess of the droplet was blotted off the grids with filter paper, then the sample was dried at room temperature.

XRD patterns of samples were recorded on a D8 Advanced diffractometer (Bruker AXS Inc., 40 kV, 30 mA) X-ray diffractometer. The samples were scanned in 2θ range of 3–70° with a step size of 0.02 and a counting time of 1.0 s using a Cu Ka radiation source (λ = 1.542 Å) and a nickel filter. Fourier transform infrared (FT-IR) spectra of nanoparticles were recorded in the range of 300–4500 cm^{-1} using a Ray Leigh Wqf-510 FT-IR spectrophotometer.

Cross-section morphology of prepared membranes was examined by SEM (KYKY-EM3200, China). To measure the top-layer thickness of membrane, four or five casual points on top-layer were selected and the average value was reported as membrane skin-layer thickness. The membrane properties are strongly affected by surface roughness [30]. Based on this fact, the surface roughness of membranes was analyzed using AFM. AFM apparatus was Dual Scope™ scanning probe-optical microscope (DME model C-21, Denmark) with AC probe in contact mode. Small squares of membranes (approximately 1 cm^2) were cut and fixed using sticky tapes on glass substrate. The membrane surface was examined in scan size 10 $\mu \times 10$ μ. Surface roughness parameters of membranes expressed in terms of S_a, S_q and S_z were obtained by SPM software (version 1.4.0.6) provided by manufacturer for quantitative analyses.

2.4.2. Hydrophilicity

In order to measure the membrane hydrophilicity, very small droplets of de-ionized water were dropped on the membrane surface in several random places, and water contact angle was measured after taking the images of droplets using a digital microscope (USB Digital Microscope 1.3 Mega Pixel Color Video Camera 400X, China). To minimize the errors, the average values of measurements were reported.

2.4.3. Water flux, porosity and mean pore radius of membranes

Water permeability of fabricated membranes was tested by pure water using a batch type, dead-end, stirred cell with an effective membrane filtration area of 12.56 cm^2 fitted with Teflon coated magnetic paddle at room temperature (20 ± 2 °C). The stirred cell fitted with a pressure gauge was pressurized with nitrogen gas to force the liquid through the membrane. To compact the membranes before measurement of pure water flux, they were pressurized using nitrogen gas at 0.45 MPa for 1 h. After compaction process, transmembrane pressure was reduced to

0.4 MPa and pure water flux was calculated using the following equation [31]:

$$\text{Permeate flux}(\text{kg/m}^2\ \text{h}) = \frac{Q}{A \times \Delta t} \quad (1)$$

where Q, A and Δt are quantity of permeate (kg), membrane area (m^2) and sampling time (h), respectively.

In order to measure the membrane porosity, the membrane sample with certain dimension was dipped in water for 24 h. Then, the surface of species was dried by filter paper and immediately weighed. After that, the membranes were dried in an oven at 50 °C for 24 h and weighed again. Overall porosity (ε) was determined by gravimetric method using the following equation [32]:

$$\varepsilon(\%) = \frac{W_w - W_d}{A' \times l \times d_w} \times 100 \quad (2)$$

where W_w, W_d, A', l and d_w are wet and dry membrane weights (g), surface area of membrane sample (cm^2), membrane thickness (cm) (measured by a digital micrometer (Mitotoyo, Japan)) and water density (0.998 g/cm^3), respectively. Moreover, membrane mean pore radius (r_m) was determined using Eq. (3) (Guerout–Elford–Ferry equation) [32,33]:

$$r_m = \sqrt{\frac{(2.9 - 1.75\varepsilon)8\eta l Q'}{\varepsilon A \Delta P}} \quad (3)$$

where η is water viscosity (8.9×10^{-4} Pa s), Q' is volumetric flow rate of permeated pure water (m^3/s), A is membrane effective surface area (m^2), and ΔP is operating pressure (0.4 MPa).

2.4.4. Cu removal tests

In order to investigate the membrane ability for filtration of solutions containing low concentrations of Cu(II) ions, a 20 mg/l aqueous $Cu(NO_3)_2$ solution was selected as feed solution. pH of copper solutions was adjusted to 5.0 because precipitation of $Cu(OH)_2$ occurs in a pH greater than 6.0. All experiments were carried out at room temperature (20 ± 2 °C) using the dead-end cell with characteristics explained in previous section. Ion removal was monitored by atomic absorption spectroscopy (Atomic Absorption Spectrophotometer PG-990 (PG Instruments Limited, UK)) of feed and permeated solutions. Copper ion removal ($R(\%)$) was calculated using Eq. (4) [31]:

$$R(\%) = (1 - (C_p/C_f)) \times 100 \quad (4)$$

where C_p and C_f are copper ion concentration (mg/l) in permeate and feed, respectively.

Finally, a membrane with the best performance in copper removal was selected to probe the reusability test using EDTA solution as chelating agent. In this case, 25 ml of 10 mM EDTA solution with pH value 10.5 was prepared. According to pK_a values of EDTA which are 1.99, 2.67, 6.16 and 10.26, Y^{4-} (the desired form of EDTA) is the dominant species of EDTA at pHs higher than 10.26. The membrane was immersed in the prepared solution and stirred for 1 h. Then, membrane was washed with plenty of de-ionized water and placed in dead-end cell to repeat Cu(II) removal test. This procedure was sequentially performed four times with duration of 120 min for each cycle of experiment.

3. Results and discussions

3.1. Fe_3O_4 based nanoparticle analyses

The modified nanoparticles were characterized by various techniques such as TEM, SEM, EDX and XRD. XRD patterns of Fe_3O_4 nanoparticles before and after silica coating (Fig. 2) clearly verify cubic spinel structure attributed to the magnetite (JCPDS No. 65-3107), and strongly proves the formation of Fe_3O_4 phase. Applying the (311) peak in Scherrer's formula, mean crystallite size was calculated about 9.5 nm [18,34]. Considering Fig. 2(b), a broad peak appeared in 20–28° confirms formation of amorphous SiO_2. Presence of amorphous layer reduced the intensity of peaks related to Fe_3O_4.

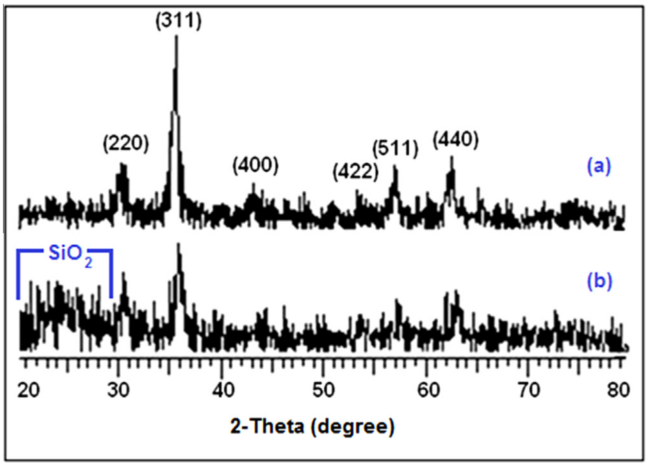

Fig. 2. XRD patterns for (a) trisodium citrate-treated Fe_3O_4 and (b) Fe_3O_4/SiO_2 nanoparticles.

Morphology of metformine and amine-modified silica coated Fe_3O_4 nanoparticles before and after surface modification was studied by TEM (Fig. 3). TEM observation indicates that trisodium citrate-treated Fe_3O_4 nanoparticles are monodispersed and have average diameter about 9.2 nm. Fe_3O_4/SiO_2-Met, -Amine nanoparticles and silica-coated Fe_3O_4 nanoparticles possess a typical core-shell structure with average size ∼40–45 nm, 35–40 nm (see Fig. 3), and ∼40 nm, respectively.

Moreover, Fig. 4 shows SEM microphotograph of Fe_3O_4/SiO_2-Met nanoparticles which proves the nanometric structure of particles. Similar result was observed in SEM microphotograph of Fe_3O_4/SiO_2-Amine nanoparticles (not shown). In addition to TEM and SEM analyses, EDX analysis for Fe_3O_4/SiO_2-Met nanoparticle (Fig. 4) confirmed the elemental composition of modified nanoparticles and existence of Si and Fe in nanoparticles. Same result for Fe_3O_4/SiO_2-Amine nanoparticles was obtained by EDX analysis indicating stable silica modification after coating nanoparticles with amine (not shown).

Silica-coating and subsequent amine and metformin functionalization of Fe_3O_4 nanoparticles can be confirmed by FT-IR spectra. Fig. 5(a) shows FT-IR spectrum of Fe_3O_4 modified with trisodium citrate. The observed peak at 579 cm^{-1} is attributed to Fe–O bond vibration. Additionally, two bands observed at 1617 and 1385 cm^{-1} are related to COO–Fe bond and confirm the formation of complex between carboxylate of citrate groups and iron ions on Fe_3O_4 nanoparticle surface. In the case of Fe_3O_4/SiO_2 nanoparticles (Fig. 5(b)), the sharp band at 1090 cm^{-1} is due to Si–O–Si anti-symmetric stretching vibration which proves the existence of a SiO_2 layer around F_3O_4 nanoparticles. Considering Fig. 5(c), metformin-modified nanoparticles shows a band appeared at 1568 cm^{-1} attributed to C=N stretching vibrations of biguanides which metformin contains it. From Fig. 5(d), the broad band at 3408 cm^{-1} is attributed to the stretching vibration of N–H bond. Additionally, the peaks appeared at 1620 cm^{-1} (bending vibration of N–H in primary amine), 806 cm^{-1} (out of plan bending vibration of N–H) and 1097 cm^{-1} (C–N stretching band) are the other verifying peaks for a primary amine formation on outer shell of nanoparticles.

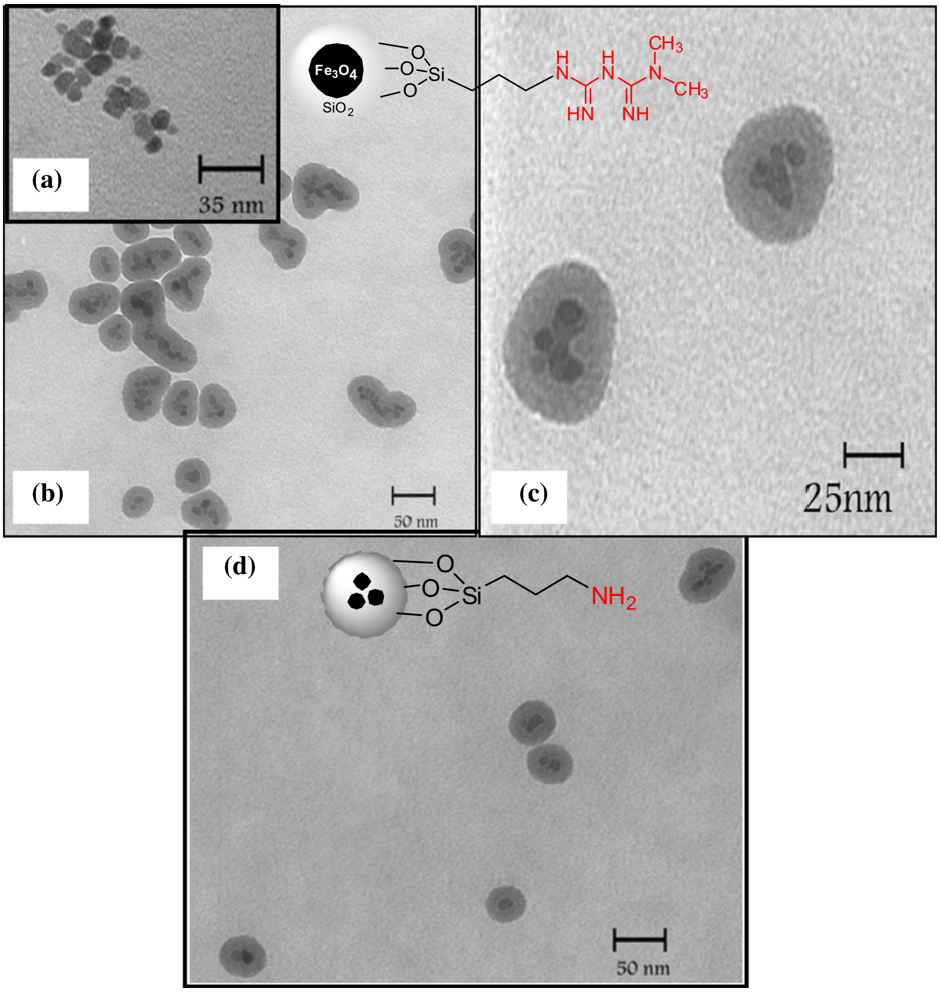

Fig. 3. TEM images of solutions containing (a) monodispersed Fe_3O_4 nanoparticles treated with trisodium citrate, (b and c) Fe_3O_4/SiO_2-Met and (d) Fe_3O_4/SiO_2-Amine nanoparticles.

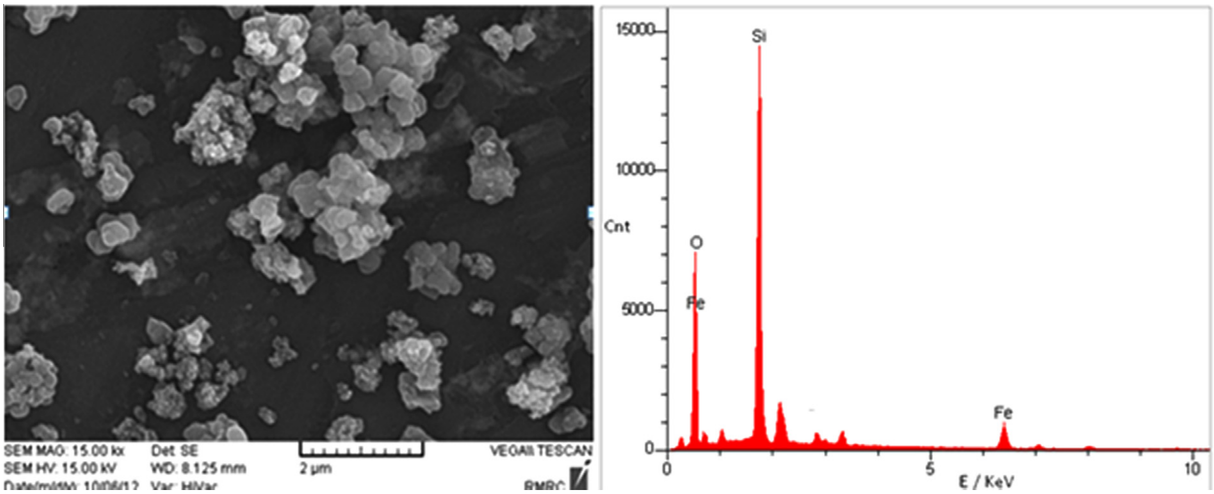

Fig. 4. (a) SEM image and (b) EDX pattern of Fe_3O_4/SiO_2-Met nanoparticles.

3.2. Pure water flux and characteristics of membranes

Results of pure water flux of membranes are shown in Fig. 6. It can be clearly seen that addition of Fe_3O_4 (pure and modified) nanoparticles resulted in an increase in the pure water permeation through the membranes compared with pristine PES membrane. This increment is in the order of PES/FeSi > PES/FeSiMet > PES/Fe > PES/FeSiAmine membranes.

Several factors involving membrane morphology (porosity, skin layer thickness and mean pore size) and hydrophilicity determine

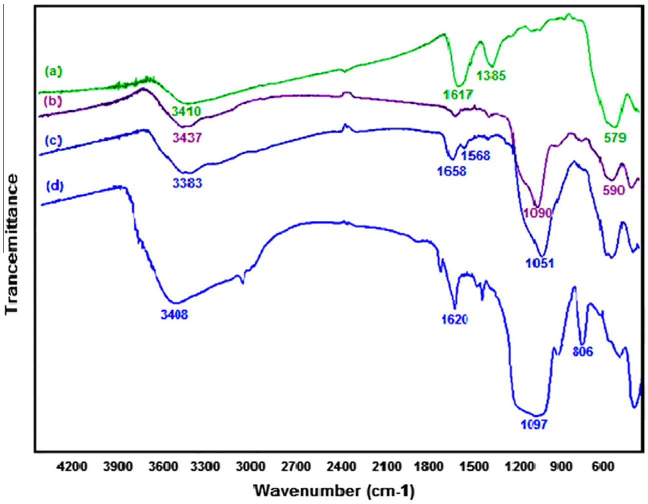

Fig. 5. FT-IR spectra of (a) Fe_3O_4 treated with trisodium citrate (b) Fe_3O_4/SiO_2, (c) Fe_3O_4/SiO_2-Met and (d) Fe_3O_4/SiO_2-Amine.

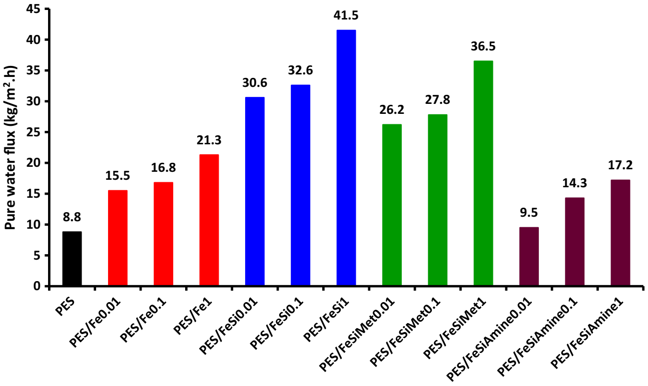

Fig. 6. Pure water flux of PES and nano-enhanced membranes.

the permeation flux through the membrane [18]. SEM cross-section images of membranes are presented in Fig. 7. Addition of different types and concentrations of Fe_3O_4 nanoparticles resulted in a growth in membrane sub-layer porosity. Moreover, sub-layer macro-voids have grown by increasing of amount of NPs in the membrane matrix. In order to prove the growth of macro-voids, image analysis software (Image J 1.48v) was employed to determine the mean size of macro-voids (see Table 3). Moreover, to confirm the increment of membrane porosity, the overall porosity information of prepared membranes is presented in Table 3 which reveals that nano-enhanced membranes offer greater void capacity and swell to a higher degree compared with PES membrane. This is attributed to the presence of nanoparticles and their effect on phase inversion kinetic i.e. the rate of membrane precipitation during replacement of solvent (DMAc) and non-solvent (water). Growing the macro-voids in sub-layer by addition of metal oxide nanoparticles into the membrane matrix has been proved before [18,31].

Moreover, as shown in Table 3, addition of NPs led to a raise in mean pore size of composite membranes. This effect facilitates water molecule penetration through the membranes and subsequently enhances the flux. Due to hydrophilicity of Fe_3O_4 (pure and modified) nanoparticles, penetration rate of water (non-solvent) into the casting solution increases with addition of nanoparticles and increasing the content during the phase inversion process. Additionally, the solvent (DMAc) diffusion rate from the membrane into the water can also increase with adding nanoparticles [35]. Due to this fact that interaction between polymer and solvent molecules is declined by obstruction of nanoparticles, solvent molecules can diffuse more easily from the polymer matrix into the coagulation bath [36]. Therefore, the average pore size and porosity of composite membranes might be higher than those of nascent PES membrane.

Water contact angle of composite membranes decreased compared to PES membrane (see Table 4). The less the water contact angle, the more the hydrophilicity. It should be noticed that iron oxide NPs tend to move to membrane surface during phase inversion process as a result of their hydrophilicity. Membrane surface is the first place contacting with water (non-solvent) during phase inversion process [18]. Comparing the images of top and bottom surface of PES and composite membranes presented in Fig. 8, the difference between the colors is clearly recognizable (particularly in membranes fabricated with 1 wt.% of NPs). The migration of NPs to top surface of membrane increases the membrane hydrophilicity compared to nascent PES membrane.

On the other hand, increasing hydrophilicity and mean pore size of membrane lead to a rise in the permeate flux. Comparing the previous study [18] in which polyaniline coated iron oxide was embedded in the membrane matrix, higher hydrophilicity of modifiers in current study resulted in superior water flux of nano-enhanced membranes. Polyaniline is much more hydrophobic than metformin and amine due to possessing aromatic hydrocarbons. Therefore, employing hydrophilic modifiers containing nucleophile functional groups for modification of iron oxide NPs is preferred to prevent permeate flux decline which was seen for PES/polyaniline/iron oxide mixed matrix membrane [18]. Considering Fig. 6, higher hydrophilicity of embedded NPs (Fe_3O_4/SiO_2 and Fe_3O_4/SiO_2-Met) offered higher water flux. PES/Fe and PES/FeSiAmine series containing NPs with lower hydrophilicity ranked the next places. The observed results are attributed to the chemical nature of NPs. Having a higher molar fraction of N atoms, Fe_3O_4/SiO_2-Met possesses significant high hydrophilicity. This effect is weakened in the case of amine in Fe_3O_4/SiO_2-Amine NP because of C_3 chain that makes it more hydrophobic. Also, SiO_2 shows higher tendency to absorb water molecules rather than Fe_3O_4 as its nature implies.

AFM surface images of PES and composite membranes are shown in Fig. 9. The surface roughness of PES membrane boosted after addition of NPs (see Table 4). More ups and downs result in higher roughness of membrane surface which might be considered as a sign for increasing surface pore size. Increasing the membrane surface roughness by adding nanoparticles might be due to the presence of NPs on the membrane surface and increasing of surface pore size [31]. However, this increment is not equal for all mixed matrix membranes prepared in this study which originates from different chemical structure and different size of embedded nanoparticles. In fact, several factors including hydrophilicity, surface pore size, bulk porosity and skin layer thickness of membranes control pure water flux of membranes. Thinner top-layer, higher bulk porosity, bigger surface pore size and more hydrophilic surface (see Tables 3 and 4) allow better water permeation through the membrane (Fig. 6).

3.3. Cu(II) removal

The previous study [18] revealed that the existence of a nucleophile group on the iron oxide surface promotes the Cu(II) adsorption efficiency of nanocomposite membrane. Hence, the basis of selection of new modified iron oxide based NPs was the increment of available nucleophile groups with various types of chemical modifiers to obtain higher copper removal efficiency with a similar mechanism. Therefore, the initial expectation was an increase in removal of Cu(II) through applying a modifier with

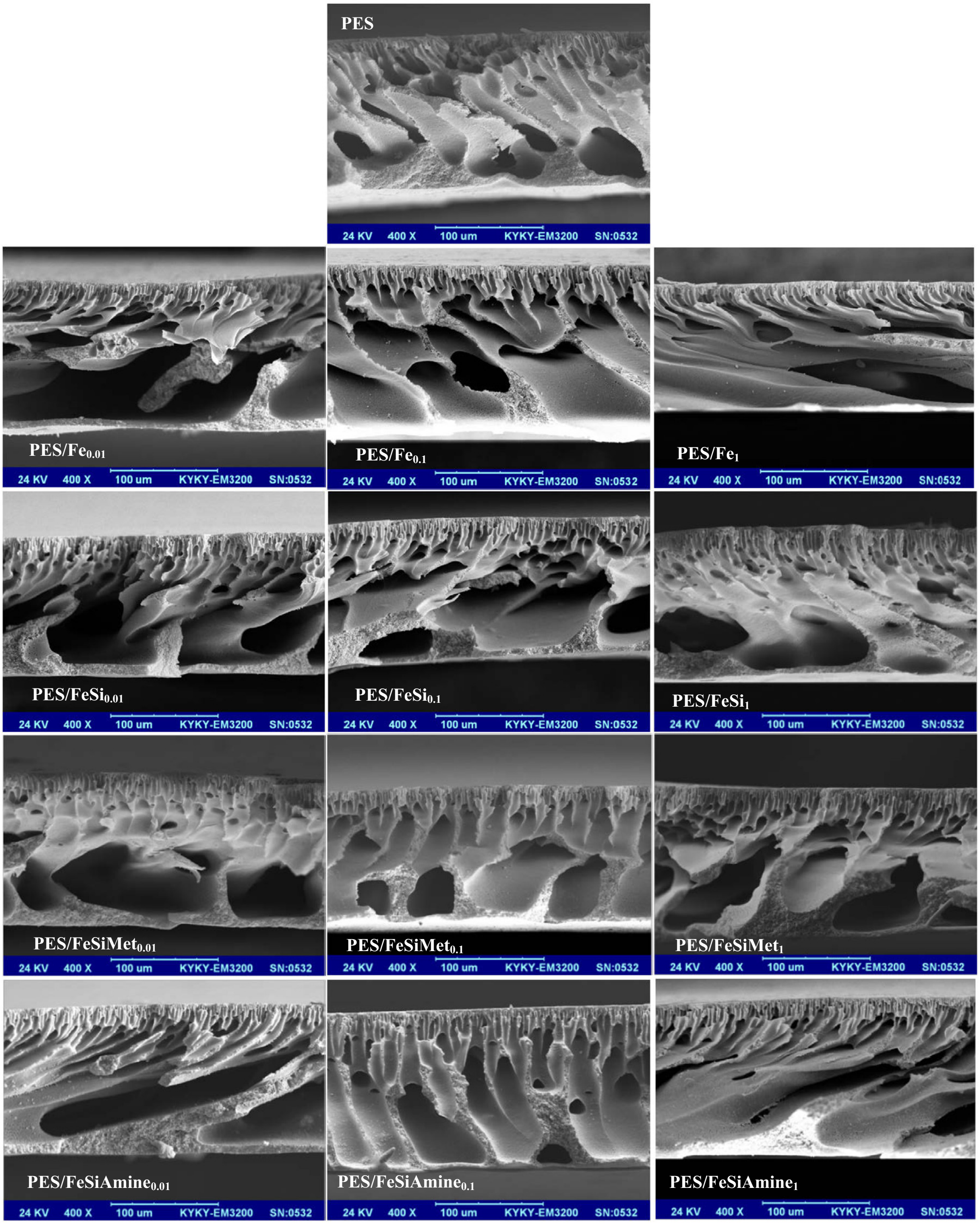

Fig. 7. SEM cross-section images of PES and nano-enhanced membranes.

higher hydrophilicity and more nucleophilic atoms. Knowing about the probable removal mechanism, investigation of copper removal efficiency would be worthy of respect. Cu(II) removal results presented in Fig. 10 strongly confirm the mentioned anticipation. Also, Fig. 11 indicates the best results of copper removal among mixed matrix membranes with each type of NPs. Higher Cu(II) removal is attributed to the membrane mixed with Fe_3O_4/SiO_2-Met NPs. The membrane enhanced with Fe_3O_4/SiO_2-Amine nanoparticles possesses the second rank in removal of Cu(II). Considering the chemical structure of these nanoparticles, there is large number of N atoms around each particle offering active adsorption sites through their lone electron pairs. Despite the higher copper removal offered by all modified membranes rather than nascent PES, membranes mixed with Fe_3O_4 and Fe_3O_4/SiO_2 NPs showed less elevation compared to membranes mixed with Fe_3O_4/SiO_2-Met and Fe_3O_4/SiO_2-Amine NPs. This proves that the functional groups play a key role in improvement of copper ion adsorption. The increment in Cu(II) removal in FeSi membranes compared to Fe series might be attributed to higher hydrophilicity of SiO_2 which allows feed solution penetrate more into the

Table 3
Mean size of macro-voids (μm), overall porosity (%), mean pore radius (nm), and skin layer thickness of membranes.

Membrane	Mean size of macro-voids (μm)	Overall porosity (%)	Mean pore radius (nm)	Skin layer thickness (nm)
PES	45.6 ± 3.1	59.3 ± 2.0	5.01 ± 0.21	659.4 ± 15.3
PES/$Fe_{0.01}$	86.8 ± 5.0	62.9 ± 2.2	5.51 ± 0.18	357.8 ± 8.1
PES/$Fe_{0.1}$	84.8 ± 6.2	74.0 ± 2.3	6.62 ± 0.11	559.9 ± 9.3
PES/Fe_1	128.0 ± 6.0	69.9 ± 2.0	6.80 ± 0.15	511.9 ± 10.5
PES/$FeSi_{0.01}$	74.8 ± 5.5	66.5 ± 2.1	8.43 ± 0.22	585.9 ± 8.5
PES/$FeSi_{0.1}$	84.3 ± 4.3	79.5 ± 2.6	7.43 ± 0.19	544.2 ± 10.1
PES/$FeSi_1$	88.7 ± 6.2	63.6 ± 2.4	10.03 ± 0.21	445.8 ± 5.9
PES/$FeSiMet_{0.01}$	94.4 ± 7.3	67.4 ± 2.3	7.72 ± 0.15	492.7 ± 6.3
PES/$FeSiMet_{0.1}$	51.7 ± 3.6	76.0 ± 2.9	7.11 ± 0.12	435.7 ± 7.1
PES/$FeSiMet_1$	59.9 ± 2.5	61.9 ± 2.2	9.80 ± 0.24	601.0 ± 6.6
PES/$FeSiAmine_{0.01}$	89.1 ± 6.4	61.1 ± 2.2	5.0 ± 0.15	378.2 ± 7.1
PES/$FeSiAmine_{0.1}$	57.0 ± 3.9	74.3 ± 2.4	5.24 ± 0.18	596.5 ± 8.7
PES/$FeSiAmine_1$	91.6 ± 7.0	66.7 ± 2.1	6.32 ± 0.20	558.8 ± 6.2

Table 4
Water contact angle (°) and roughness parameters of membranes.

Membrane	WCA (°)	Roughness parameters		
		S_a (nm)	S_q (nm)	S_z (nm)
PES	78 ± 0.5	13.3 ± 0.4	16.6 ± 0.6	103 ± 2.4
PES/$Fe_{0.1}$	72 ± 0.8	22.4 ± 4.5	50.7 ± 3.6	298 ± 52.5
PES/$FeSi_{0.1}$	67 ± 0.5	18.9 ± 3.5	38.3 ± 6.0	276 ± 45.1
PES/$FeSiMet_{0.1}$	69 ± 0.7	17.8 ± 0.4	38.6 ± 1.5	232 ± 22.5
PES/$FeSiAmine_{0.1}$	75 ± 0.4	17.4 ± 2.9	29.5 ± 5.7	205 ± 66.7

nanoparticles and adsorb larger number of Cu(II) ions. On the other hand, a higher dispersion of nanoparticles due to higher hydrophilicity of Fe_3O_4/SiO_2 nanoparticles leads to increase in the number of available adsorption sites on the membrane surface. Consideration of roughness parameters is a useful method in determination of dispersion quality of NPs on the membrane surface. Given the data tabulated in Table 4, although the addition of NPs increases the surface roughness, better dispersion of nanoparticles might compensate the increment of roughness [18]. Therefore, PES/$FeSi_{0.1}$ with S_a value lower than PES/$Fe_{0.1}$ (18.9 nm vs. 22.4 nm) offers higher dispersion of NPs i.e. less agglomeration. This phenomenon results in formation of more available active sites for adsorption of copper ions.

Results in Fig. 10 also demonstrate that applying various amounts of nanoparticles can affect the membrane performance. Whereas the membranes act as an adsorptive barrier due to chemical structure of NPs, the increment of available active sites and higher surface area (well dispersed NPs) influences the cation removal efficiency. In each series of membranes mixed with different concentrations of NPs, a different trend of Cu(II) removal can be observed by increasing/decreasing the amount of NPs in membrane matrix. In PES/Fe membranes, higher amount of NPs resulted in an enhancement of copper removal capability which supports this fact that unmodified Fe_3O_4 NPs have weaker adsorption ability. This means that a higher amount of Fe_3O_4 NPs are needed to have a considerable increment of copper removal compared with nascent PES membrane. In PES/FeSi membranes, the aforementioned effect is much weaker. It can be seen that there is no significant difference between Cu(II) removal of PES/$FeSi_{0.01}$ and PES/$FeSi_{0.1}$. Indeed, bigger particle size of core-shell structured Fe_3O_4/SiO_2 NPs [34] prevents increment of available adsorption sites by adding more NPs. This effect is intensified at the case of PES/FeSiMet and PES/FeSiAmine series containing NPs with bigger size. Compared with smaller nanoparticles, bigger size of nanoparticles prevents their efficient migration towards membrane top surface. Moreover, when a specific amount of nanoparticles is considered, the number of particles with smaller size is more than that with bigger size. Thus, due to higher number of smaller particles, it is obvious that the effect of smaller nanoparticles in a nanocomposite is more significant than bigger ones. To put in other words, the effectiveness of adding more amounts of nanoparticles is limited by nanoparticle size. An evidence for this fact is color of prepared membranes illustrated in Fig. 8. Similar findings were also presented in another study [37].

In order to introduce a nano-enhanced membrane with the best performance in decreasing the copper concentration of effluents, the simultaneous consideration of permeate flux, copper removal and employed NPs amount are needed. Fig. 12 demonstrates the flux versus removal percent for each fabricated membrane. As it

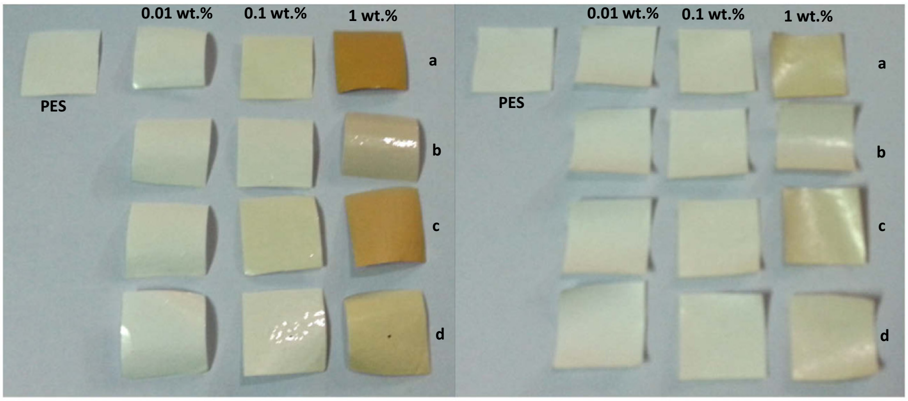

Fig. 8. Images of top (left hand) and bottom (right hand) surface of PES and nano-enhanced membranes fabricated with different concentrations of (a) Fe_3O_4, (b) Fe_3O_4/SiO_2, (c) Fe_3O_4/SiO_2-Met and (d) Fe_3O_4/SiO_2-Amine nanoparticles.

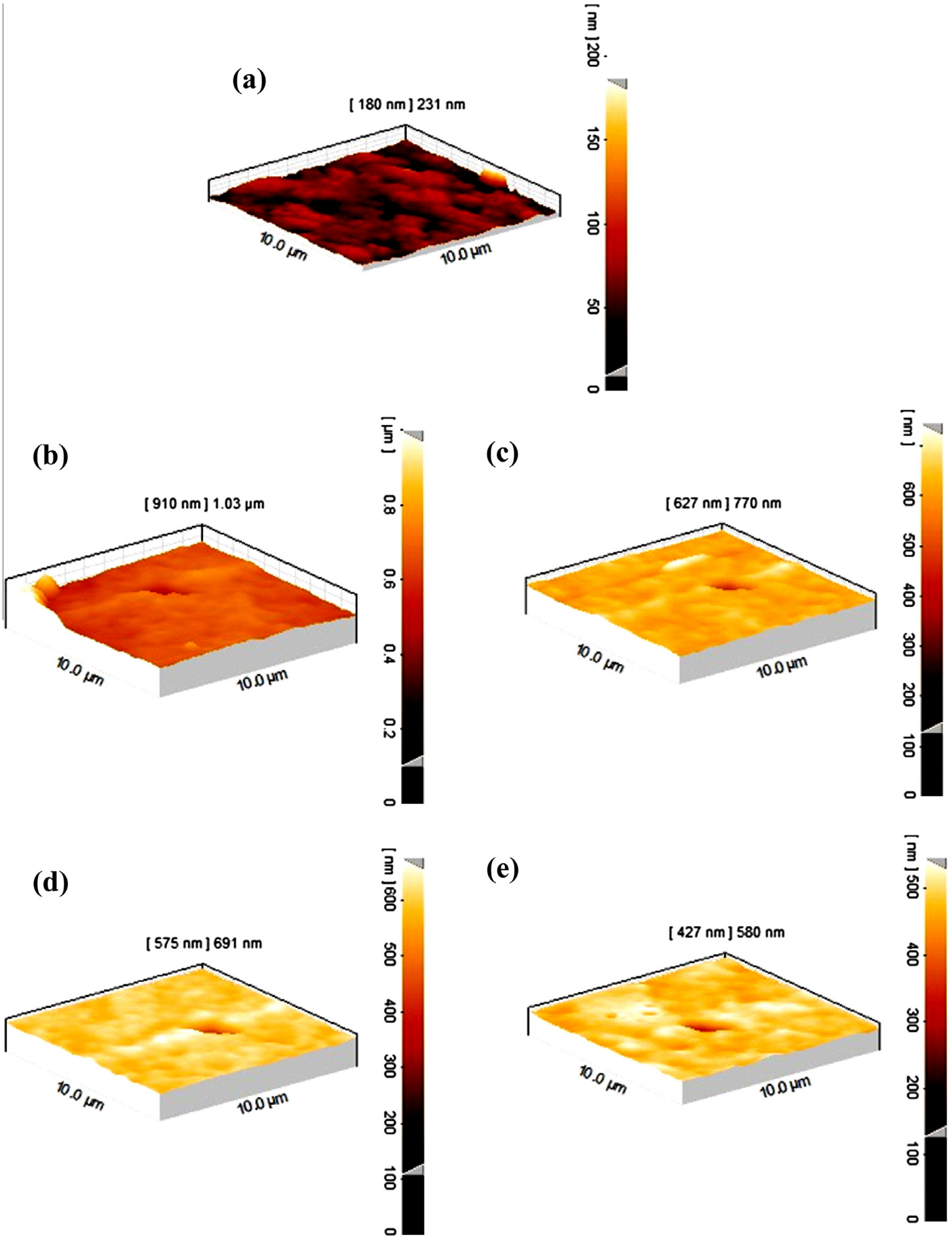

Fig. 9. AFM images of (a) PES, (b) PES/$Fe_{0.1}$, (c) PES/$FeSi_{0.1}$, (d) PES/$FeSiAmine_{0.1}$ and (e) PES/$FeSiAMet_{0.1}$.

can be seen, PES/$FeSiMet_{0.1}$ presents the highest copper removal, a moderate permeate flux as well as an acceptable low consumption of NPs.

Given the results of copper removal, the enhancement in Cu removal is observable in this study compared to the previous work [18]. This increment might be due to more adsorption sites (N atoms) of modified NPs offered by metformin compared with polyaniline. Moreover, hydrophilicity of Fe_3O_4/SiO_2-Met NPs causes better dispersion of nanoparticles in the membrane matrix as well as on the membrane surface during phase inversion process. Also, the hydrophilicity of new modified NPs may reinforce the migration of NPs toward the membrane surface and increase the available active sites on the membrane surface. This leads to increment of adsorption ability of membrane. The more the adsorption sites on the membrane surface, the more the capability of membrane in adsorption of copper.

It should be noticed that the membrane acts as an adsorptive filter not as an adsorbent media i.e. there is a complicated filtration–adsorption mechanism that allows the ion removal efficiency to be stable after a distinct period. Hence, Cu(II) removal capability

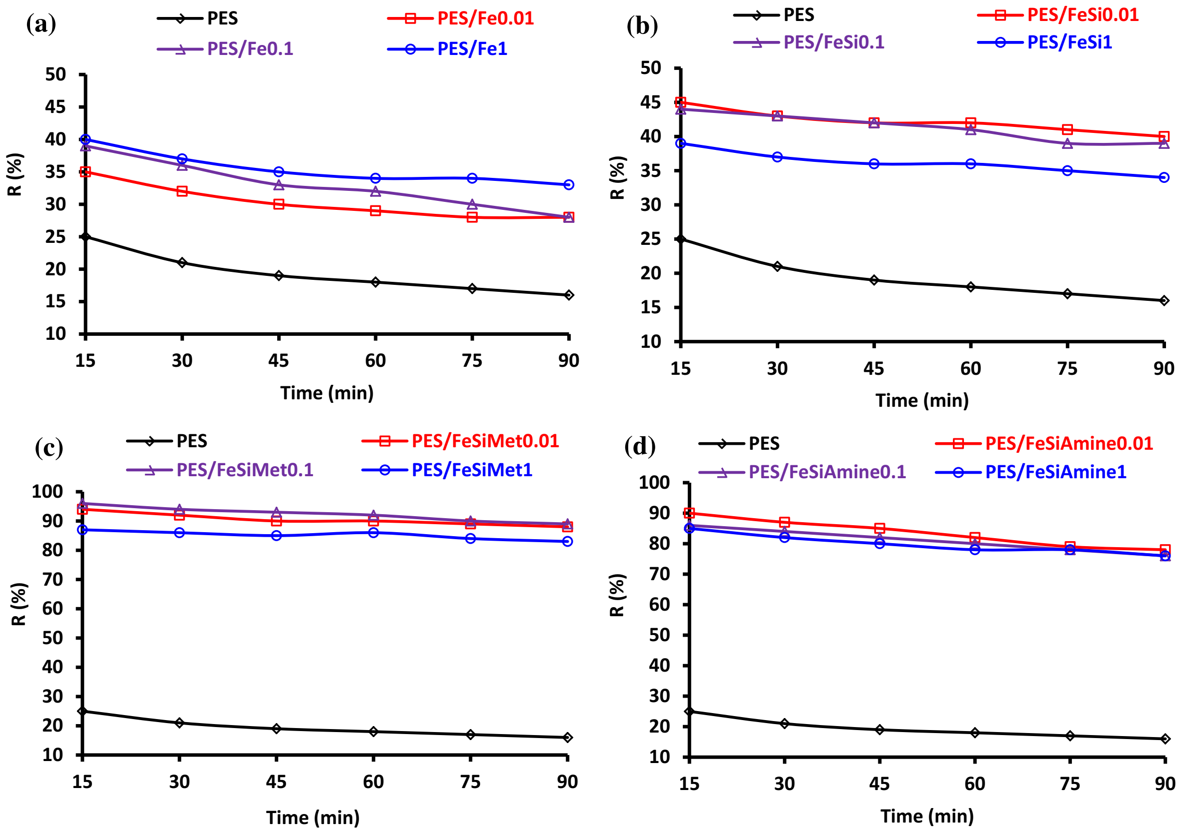

Fig. 10. Copper ion removal versus time using pristine PES and nano-enhanced membranes prepared with different concentrations of (a) Fe_3O_4, (b) Fe_3O_4/SiO_2, (c) Fe_3O_4/SiO_2-Met and (d) Fe_3O_4/SiO_2-Amine nanoparticles.

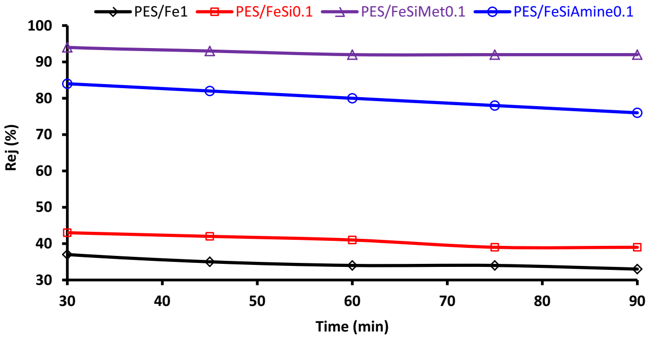

Fig. 11. Comparison of copper ion removal using nano-enhanced membranes.

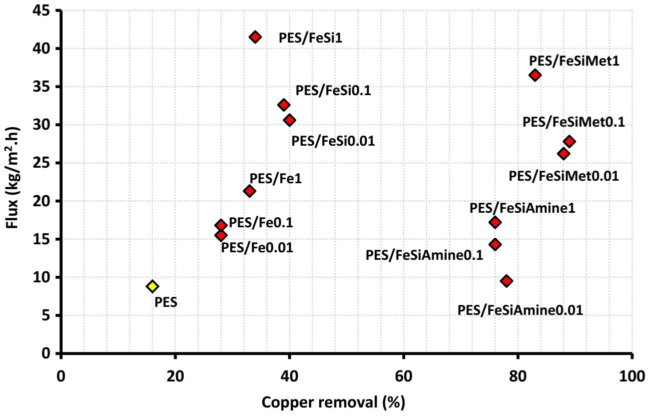

Fig. 12. Flux versus copper removal for nano-enhanced membranes after passage of 90 min of test commencement.

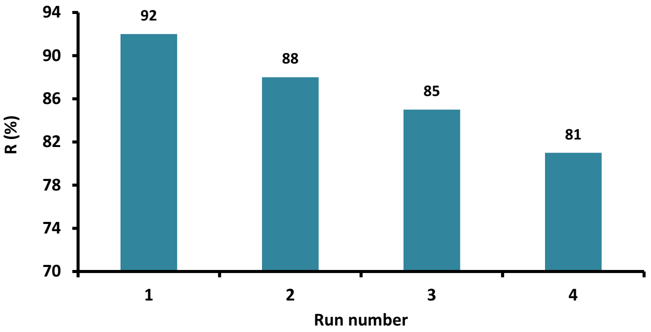

Fig. 13. Reusability of PES/FeSiMet$_{0.1}$ for four sequential runs.

was focused more than adsorption capacity. This would be closer to definition of membranes.

3.4. Membrane reusability

As discussed before, nano-enhanced membranes removed the copper ions during an adsorption process on the active sites of blended NPs. The reversibility of adsorption process controls the reusability of prepared membranes. Hence, the reusability test was performed by the same approach as it was introduced in the previous study [18]. For this purpose, the PES/FeSi-Met$_{0.1}$ membrane with the highest efficiency in copper removal was selected. Fig. 13 illustrates the cation removal for four sequential runs. Results show that a reduction rate of about 4% achieves after each run of copper removal/regeneration test. This proves an acceptable reusability of nano-enhanced membranes to be applied for removal of copper ions after being used for several times.

4. Conclusion

Nano-enhanced polymeric membrane was prepared by addition of different types of modified iron oxide nanoparticles. Fe_3O_4 nanoparticles were coated by silica, metformine and amine, and then employed for fabrication of PES mixed matrix membranes. The prepared membranes were characterized by morphology (SEM and AFM images), hydrophilicity, mean pore size radius, porosity, pure water flux and copper removal. The modified iron oxide nanoparticles applied in this study are well comparable with previous study [18]. This work showed a novel idea to increase iron oxide/PES mixed matrix membrane permeability by applying more hydrophilic modifiers. Results are summarized as follow:

(1) Blending surface modified Fe_3O_4 nanoparticles with PES polymer led to an increase in hydrophilicity and pure water flux of membrane. Iron oxide nanoparticles affected on the mean pore radius and the overall porosity of membranes.
(2) SEM cross-section images of membranes showed that presence of nanoparticles in the membrane matrix resulted in a growth in membrane sub-layer porosity. Moreover, surface roughness of PES membrane increased after addition of NPs.
(3) All nano-enhanced membranes revealed higher efficiency in Cu(II) removal as a result of high hydrophilicity and nucleophilic groups of the nanoparticles. It was revealed that dispersion of NPs is also responsible for efficient removal of Cu(II) due to both type and concentration of applied NPs.
(4) The membrane fabricated with 0.1 wt.% metformine-modified silica coated Fe_3O_4 nanoparticle showed the highest amount of copper removal (about 92%) due to large number of N atoms around each particle offering active adsorption sites through their lone electron pairs. Repetition of removal tests confirmed excellent reusability as well as durability of this membrane during four sequential filtration tests.

As an overall analysis, employing appropriate organic/inorganic modifiers for inorganic nanoparticles like iron oxide might promote the characteristics of a polymeric nano-enhanced membrane mixed with nanoparticles. Also, proper modification of NPs leads to a decrement in the quantity of the applied NPs for achieving an acceptable permeate flux and contaminant removal.

References

[1] P.C. Eck, L. Wilson, Copper Toxicity, Eck Institute of Applied Nutrition and Bioenergetics, Ltd., 1989.
[2] S.M. Reichman, The Responses of Plants to Metal Toxicity: A review focusing on Copper, Manganese and Zinc, Australian Minerals & Energy Environment Foundation, Melbourne, 2002.
[3] J. Garcia-Leston, J. Mendez, E. Pasaro, B. Laffon, Genotoxic effects of lead: an updated review, Environ. Int. 36 (2010) 623–636.
[4] M. Hua, S. Zhang, B. Pan, W. Zhang, L. Lv, Q. Zhang, Heavy metal removal from water/wastewater by nanosized metal oxides: a review, J. Hazard. Mater. 211–212 (2012) 317–331.
[5] S. Ona, E. Toorisaka, M. Hirata, T. Hano, Adsorption and toxicity of heavy metals on activated sludge, Sci. Asia. 36 (2010) 204–209.
[6] Z. Ren, W. Zhang, H. Meng, J. Liu, S. Wang, Extraction separation of Cu(II) and Co(II) from sulfuric solutions by hollow fiber renewal liquid membrane, J. Membr. Sci. 365 (2010) 260–268.
[7] Y. Ku, S. Chen, W. Wang, Effect of solution composition on the removal of copper ions by nanofiltration, Sep. Purif. Technol. 43 (2005) 135–142.
[8] C. Tizaoui, S.D. Rachmawati, N. Hilal, The removal of copper in water using manganese activated saturated and unsaturated sand filters, Chem. Eng. J. 209 (2012) 334–344.
[9] M.A. AbuDalo, S. Nevostrueva, M.T. Hernandez, Enhanced copper (II) removal from acidic water by granular activated carbon impregnated with carboxybenzotriazole, APCBEE Proc. 5 (2013) 64–68.
[10] P. SenthilKumar, S. Ramalingam, V. Sathyaselvabala, S. Dinesh Kirupha, S. Sivanesan, Removal of copper (II) ions from aqueous solution by adsorption using cashew nut shell, Desalination 266 (2011) 63–71.
[11] H. Aydın, Y. Bulut, Ç. Yerlikaya, Removal of copper (II) from aqueous solution by adsorption onto low-cost adsorbents, J. Environ. Manage. 87 (2008) 37–45.
[12] K. Jasiewicz, R. Pietrzak, The influence of pore generating agent on the efficiency of copper and iron ions removal from liquid phase by polyethersulfone membranes, Chem. Eng. J. 228 (2013) 449–454.
[13] C. Magnenet, F.E. Jurin, S. Lakard, C.C. Buron, B. Lakard, Polyelectrolyte modification of ultrafiltration membrane for removal of copper ions, Colloids Surf. A 435 (2013) 170–177.
[14] C. Liu, R. Bai, Adsorptive removal of copper ions with highly porous chitosan/cellulose acetate blend hollow fiber membranes, J. Membr. Sci. 284 (2006) 313–322.
[15] W. Han, C. Liu, R. Bai, A novel method to prepare high chitosan content blend hollow fiber membranes using a non-acidic dope solvent for highly enhanced adsorptive performance, J. Membr. Sci. 302 (2007) 150–159.
[16] A.G. Boricha, Z.V.P. Murthy, Acrylonitrile butadiene styrene/chitosan blend membranes: preparation, characterization and performance for the separation of heavy metals, J. Membr. Sci. 339 (2009) 239–249.
[17] Z. Cheng, X. Liu, M. Han, W. Ma, Adsorption kinetic character of copper ions onto a modified chitosan transparent thin membrane from aqueous solution, J. Hazard. Mater. 182 (2010) 408–415.
[18] P. Daraei, S.S. Madaeni, N. Ghaemi, E. Salehi, M.A. Khadivi, R. Moradian, B. Astinchap, Novel polyethersulfone nanocomposite membrane prepared by PANI/Fe_3O_4 nanoparticles with enhanced performance for Cu(II) removal from water, J. Membr. Sci. 415–416 (2012) 250–259.
[19] L.Y. Ng, A.W. Mohammad, C.P. Leo, N. Hilal, Polymeric membranes incorporated with metal/metal oxide nanoparticles: a comprehensive review, Desalination 308 (2013) 15–33.
[20] P. Sabbatini, F. Yrazu, F. Rossi, G. Thern, A. Marajofsky, M.M. Fidalgo de Cortalezzi, Fabrication and characterization of iron oxide ceramic membranes for arsenic removal, Water Res. 44 (2010) 5702–5712.
[21] H. Park, H. Choi, As(III) removal by hybrid reactive membrane process combined with ozonation, Water Res. 45 (2011) 1933–1940.
[22] A. Gholami, A.R. Moghadassi, S.M. Hosseini, S. Shabani, F. Gholami, Preparation and characterization of polyvinyl chloride based nanocomposite nanofiltration-membrane modified by iron oxide nanoparticles for lead removal from water, J. Ind. Eng. Chem. 20 (2014) 1517–1522.
[23] G.R. Xu, J.N. Wang, C.J. Li, Preparation of hierarchically nanofibrous membrane and its high adaptability in hexavalent chromium removal from water, Chem. Eng. J. 198–199 (2012) 310–317.
[24] C.J. Li, Y.J. Li, J.N. Wang, J. Cheng, PA6@FexOy nanofibrous membrane preparation and its strong Cr(VI)-removal performance, Chem. Eng. J. 220 (2013) 294–301.
[25] N.A. Weerasekara, K.H. Choo, S.J. Choi, Metal oxide enhanced microfiltration for the selective removal of Co and Sr ions from nuclear laundry wastewater, J. Membr. Sci. 447 (2013) 87–95.
[26] D. Yang, J. Hu, S. Fu, Controlled synthesis of magnetite-silica nanocomposites via a seeded sol–gel approach, J. Phys. Chem. C 113 (2009) 7646–7651.
[27] W. Stöber, A. Fink, E. Bohn, Controlled growth of monodisperse silica spheres in the micron size range, J. Colloid Interface Sci. 26 (1968) 62–69.
[28] T. Zeng, L. Yang, R. Hudson, G. Song, A.R. Moores, C.J. Li, Fe_3O_4 nanoparticle-supported copper (I) pybox catalyst: magnetically recoverable catalyst for enantioselective direct-addition of terminal alkynes to imines, Org. Lett. 13 (2011) 442–445.
[29] J.H. Jang, H.B. Lim, Characterization and analytical application of surface modified magnetic nanoparticles, Microchem. J. 94 (2010) 148–158.
[30] P. Daraei, S.S. Madaeni, N. Ghaemi, H. Ahmadi Monfared, M.A. Khadivi, Fabrication of PES nanofiltration membrane by simultaneous use of multi-walled carbon nanotube and surface graft polymerization method: comparison of MWCNT and PAA modified MWCNT, Sep. Purif. Technol. 104 (2013) 32–34.
[31] N. Ghaemi, S.S. Madaeni, A. Alizadeh, H. Rajabi, P. Daraei, Preparation, characterization and performance of polyethersulfone/organically modified montmorillonite nanocomposite membranes in removal of pesticides, J. Membr. Sci. 382 (2011) 135–147.
[32] J.F. Li, Z.L. Xu, H. Yang, L.Y. Yu, M. Liu, Effect of TiO_2 nanoparticles on the surface morphology and performance of microporous PES membrane, Appl. Surf. Sci. 255 (2009) 4725–4732.
[33] N.A.A. Hamid, A.F. Ismail, T. Matsuura, A.W. Zularisam, W.J. Lau, E. Yuliwati, M.S. Abdullah, Morphological and separation performance study of polysulfone/titanium dioxide (PSF/TiO_2) ultrafiltration membranes for humic acid removal, Desalination 273 (2011) 85–92.
[34] A. Alizadeh, M.M. Khodaei, M. Beygzadeh, D. Kordestani, M. Feyzi, Biguanide-functionalized Fe_3O_4/SiO_2 magnetic nanoparticles: an efficient heterogeneous organosuperbase catalyst for various organic transformations in aqueous media, Bull. Korean Chem. Soc. 33 (8) (2012) 2546–2552.
[35] T.H. Bae, T.M. Tak, Effect of TiO_2 nanoparticles on fouling mitigation of ultrafiltration membranes for activated sludge filtration, J. Membr. Sci. 249 (2005) 1–8.
[36] V. Vatanpour, S.S. Madaeni, A.R. Khataee, S. Zinadini, H. Ahmadi Monfared, E. Salehi, TiO_2 embedded mixed matrix PES nanocomposite membranes: influence of different sizes and types of nanoparticles on antifouling and performance, Desalination 292 (2012) 19–29.
[37] P. Daraei, S.S. Madaeni, N. Ghaemi, M.A. Khadivi, B. Astinchap, R. Moradian, Enhancing antifouling capability of PES membrane via mixing with various types of polymer modified multi-walled carbon nanotube, J. Membr. Sci. 444 (2013) 184–191.